Journal of Hazardous Materials 423 (2022) 126998

Contents lists available at ScienceDirect

Journal of Hazardous Materials

journal homepage: www.elsevier.com/locate/jhazmat

Enhanced catalytic sulfamethoxazole degradation via peroxymonosulfate activation over amorphous $CoS_x@SiO_2$ nanocages derived from ZIF-67

Fei Wang [a,b], Huifen Fu [a,b,*], Fu-Xue Wang [a,b], Xiu-Wu Zhang [a,b], Peng Wang [a,b], Chen Zhao [a,b], Chong-Chen Wang [a,b,*]

[a] Beijing Key Laboratory of Functional Materials for Building Structure and Environment Remediation, Beijing University of Civil Engineering and Architecture, Beijing 100044, China

[b] Beijing Energy Conservation & Sustainable Urban and Rural Development Provincial and Ministry Co-construction Collaboration Innovation Center, Beijing University of Civil Engineering and Architecture, Beijing 100044, China

ARTICLE INFO

Editor: Dr. B. Lee

Keywords:
Sulfamethoxazole
Amorphous $CoS_x@SiO_2$
Peroxymonosulfate
Advanced oxidation process
Metal-organic frameworks

ABSTRACT

In this work, the amorphous $CoS_x@SiO_2$ nanocages were hydrothermally synthesized by sulfurizing ZIF-67@SiO_2 in the presence of thioacetamide (TAA). The catalytic performances of $CoS_x@SiO_2$ nanocages as heterogeneous catalysts to activate peroxymonosulfate (PMS) for the sulfamethoxazole (SMX) degradation were systematically investigated. 100% SMX was degraded within 6 min in $CoS_x@SiO_2$/PMS system, indicating that the amorphous $CoS_x@SiO_2$ nanocages exhibited outstanding sulfate radical-advanced oxidation process (SR-AOP) activity toward SMX degradation due to the regeneration of Co^{2+} by surficial sulfur species like S^{2-}/S_2^{2-}. The effects of PMS dosages, initial pH, SMX concentrations and co-existing ions on SMX degradation efficiency were explored in detail. The SMX removal efficiency was obviously improved in the simulated wastewater containing chloride ions (Cl^-) and low-concentration bicarbonate ions (HCO_3^-). The residual PMS and the generated sulfate radical ($SO_4\cdot^-$) were determined quantitatively in $CoS_x@SiO_2$/PMS system. A possible mechanism in $CoS_x@SiO_2$/PMS system was proposed based on the results of quenching experiments, X-ray photoelectron spectroscopy (XPS) analysis, electrochemical tests, and electron spin resonance (ESR). The $CoS_x@SiO_2$ exhibited good stability and reusability, in which 100% SMX removal was achieved even after five consecutive cycles. This work provided a strategy for regulating the stability of cobalt-based catalyst for efficient pollutant degradation by PMS activation.

1. Introduction

Up to now, antibiotics are widely used to treat human and animal infectious (Liu et al., 2021). Sulfamethoxazole (SMX), an important category of sulfonamide antibiotics, has been frequently detected in various aquatic environment with the concentrations from 0.01 to 2.0 μg/L (Yan et al., 2018). Although the detected concentration of SMX is low, it would cause serious harm to the environment. Traditional wastewater treatment processes like activated sludge cannot remove SMX completely (Zhao et al., 2021; Chen et al., 2021). Therefore, developing economical and effective techniques for SMX removal from natural water is urgent.

In recent years, advanced oxidation processes (AOPs) have attracted people's attention because it can generate highly active radicals ($SO_4\cdot^-$, ·OH, $O_2\cdot^-$, etc.) and effectively degrade antibiotic pollutants (Oh et al., 2016; Ji et al., 2021). Among all AOPs, the sulfate-based advanced oxidation process (SR-AOP), as a powerful technology, has aroused widespread attention due to its excellent degradation efficiency for organic pollutants (Zhu et al., 2019; Hammouda et al., 2018). The sulfate radical ($SO_4\cdot^-$) can be generated from peroxymonosulfate (PMS) and peroxydisulfate (PDS) activation with the help of heating, UV light, ultrasound, catalyst or the combination of the above-mentioned approaches (Lee et al., 2020; Ji et al., 2016; Dong et al., 2021). Some heterogeneous catalysts containing transition metal ions like Co^{2+}, Fe^{2+}, Cu^{2+}, Mo^{4+}, Mn^{2+} and Ce^{3+} can activate PMS/PDS to degrade pollutants effectively in the wastewater, in which the Co^{2+}-based heterogeneous catalysts exhibited the best activation performances (Li et al., 2016; Duan et al., 2018; Yi et al., 2020; Du et al., 2020). Fan et al. found that Co_3O_4 activated PMS system could completely degrade atrazine within 15 min (Fan et al., 2017). Wang et al. used Co_9S_8@biochar doped with S

* Corresponding authors at: Beijing Key Laboratory of Functional Materials for Building Structure and Environment Remediation, Beijing University of Civil Engineering and Architecture, Beijing 100044, China.

E-mail addresses: fuhuifen@bucea.edu.cn (H. Fu), wangchongchen@bucea.edu.cn, chongchenwang@126.com (C.-C. Wang).

https://doi.org/10.1016/j.jhazmat.2021.126998
Received 28 June 2021; Received in revised form 16 August 2021; Accepted 19 August 2021
Available online 21 August 2021

and N to accomplish 100% SMX decomposition within 10 min by activating PMS (Wang and Wang, 2020). In recent years, metal sulfide materials have attracted more attention due to their high removal efficiency for pollutants by activating PMS or PDS. Ding et al. reported the synthesis of CoS via hydrothermal method by using $CoCl_2{\cdot}6H_2O$ and thiourea, and CoS presented the outstanding removal efficiency for bisphenol A by PMS activation (Ding et al., 2020). The metal sulfides synthesized by above-stated methods exhibited excellent catalytic performance, however, the morphology and specific surface area of the as-synthesized products were difficult to control and tune. Therefore, it was essential to synthesize metal sulfides catalyst with large specific surface area and special morphology.

Metal-organic frameworks (MOFs) have attracted increasing attentions due to their merits like large surface area, inherent porous structure and adjustable morphology, which were widely investigated in gas separation (Rodenas et al., 2015), catalysis (including photocatalysis) (Wang et al., 2016), drug delivery (Lazaro and Forgan, 2019) and fluorescent sensing (Stassen et al., 2017). In recent years, MOF-derivatives have attracted intense interests due to that they can maintain the advantages like ultra-high surface area, high porosity, adjustable pore size and so on (Zhan et al., 2019; Li et al., 2020). MOF-derived porous materials have been adopted as excellent heterogeneous catalysts for SR-AOP (Jiang et al., 2020). ZIF-67 was the most reported template to construct Co-based catalyst for PMS activation (Wu et al., 2020). Although the derivatives from ZIF-67 displayed outstanding SR-AOP catalytic performance for organic pollutants degradation, the high Co leaching set critical limit to its practical applications (Wu et al., 2020).

In this study, the amorphous SiO_2 was introduced on the surface of CoS_x particles to overcome the above-mentioned disadvantages due to that SiO_2 with mesoporous structures and good stability has widely been studied for the various catalytic processes (Li et al., 2021). The amorphous $CoS_x@SiO_2$ nanocages were synthesized from ZIF-67@SiO_2 as precursor (as shown in Scheme 1), which was further used as SR-AOP catalyst to degrade SMX in aqueous solution. The generation mechanism of the reactive oxygen species (ROSs) like $SO_4{\cdot}^-$, ·OH and $^1O_2$ as well as the roles of sulfur species/metal cobalt ions in this SR-AOPs system were proposed and verified. It was expected that this work will provide a new strategy to stabilize catalysts in practical wastewater treatment.

2. Experimental

The reagents, instruments, and the corresponding test and characterization methods are provided in the Supplementary Information (SI).

2.1. Synthesis of ZIF-67 and ZIF-67@SiO_2 nanoparticles

ZIF-67@SiO_2 nanoparticles were prepared following the previous literature (Zhang et al., 2018). Typically, 5.4 g 2-methylimidazole, 0.35 g $Co(NO_3)_2{\cdot}6H_2O$ and 0.75 mL tetraethyl orthosilicate (TEOS) were added in 75.0 mL ultra-pure water. After stirring at room temperature for 3 h, the ZIF-67@SiO_2 was obtained by centrifuging, washing and drying. The pristine ZIF-67 was also prepared using the identical procedure except for without adding TEOS as silicate source.

2.2. Synthesis of $CoS_x@SiO_2$ nanocages

The rhombic dodecahedral ZIF-67@SiO_2 was hydrothermally sulfurized by thioacetamide (TAA) to form $CoS_x@SiO_2$ nanoparticles. 0.1 g as-prepared ZIF-67@SiO_2 and 0.4 g TAA were dispersed into 15.0 mL ethanol for obtain suspension solution, which was transferred into a 25.0 mL Teflon-lined autoclave and heated at 120 °C for 4 h. After cooling down to room temperature, the $CoS_x@SiO_2$ was collected by centrifuging, washing and drying. The individual CoS_x was also prepared using the same procedure, in which ZIF-67@SiO_2 was replaced by pristine ZIF-67 as precursor.

2.3. Catalytic SR-AOP activity of $CoS_x@SiO_2$

All experiments were conducted in the dark condition. The catalytic performance of $CoS_x@SiO_2$ was evaluated by degrading selected SMX as contaminant model. All the degradation experiments were conducted in a 60.0 mL reactor containing 50.0 mL of SMX solution (5.0 mg/L) with a constant stirring of 200 rpm under room temperature. Typically, the pH values ranging from 2.0 to 10.0 of the targeted solution were adjusted with H_2SO_4 or NaOH solutions with suitable concentrations. 10 mg $CoS_x@SiO_2$ catalyst and 0.2 mM PMS were added into the reactor to initiate the SMX degradation experiment. 1.5 mL SMX solution was filtrated from the reactor by the syringe with 0.22 μm PTFE filter at pre-set time intervals, which was immediately quenched with 10 μL methanol for further determination. The residual SMX concentrations were determined by an ultra-high performance liquid chromatography (UHPLC, Thermo Scientific Vanquish Flex). As well, the TOC removal efficiency was also detected by a TOC analyzer (multi-N/C 3100, Analytik Jena AG) to quantitatively determine the materialization during the SR-AOP procedure.

2.4. Quantification of $SO_4{\cdot}^-$ and residual PMS

The generated $SO_4{\cdot}^-$ radicals were quantified by detecting 4-benzoquinone (BQ) that was produced from the reaction of *p*–hydroxybenzoic acid (HBA) and $SO_4{\cdot}^-$ (Oh et al., 2017). Briefly, specific molar ratio of HBA and PMS were added into 60.0 mL reaction beaker with 50.0 mL

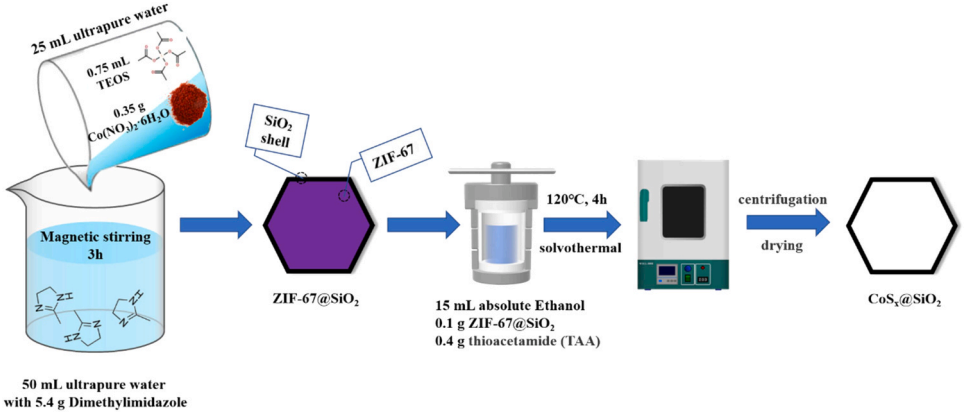

Scheme 1. Synthetic fabrication process illustration of $CoS_x@SiO_2$.

deionized water, in which $CoS_x@SiO_2$ was added as AOPs catalyst. At pre-set time interval, 1.5 mL sample was taken out and filtered by 0.22 μm PTFE filter. Meanwhile, the excessive methanol (10 μL) was immediately added to quench ROSs. The molar ratios of HBA:PMS were varied between 1:1–6:1. The formed BQ, as a stable byproduct, can be detected by UHPLC, in which the wavelength of the UV detector was set as 246 nm. Finally, the $SO_4^{\cdot -}$ concentrations were calculated based on the stoichiometric ratio of $SO_4^{\cdot -}$ to BQ.

The quantification of residual PMS was carried out. Firstly, 0.5 mL solution was taken out and mixed with 4.5 mL 1.11 g/L KI aqueous solution. The mixed solution was shaken for 30 min to ensure the complete reaction between I^- and HSO_5^- to produce I_3^- (Eqs. 1 and 2). The I_3^- concentration, proportional to PMS, was determined at λ_{max} = 352 nm by UV–vis spectrophotometer (Oh et al., 2014; Yan et al., 2019).

$$2I^- + HSO_5^- + 2\,H^+ \rightarrow HSO_4^- + I_2 + H_2O \quad (1)$$

$$I_2 + I^- \rightarrow I_3^- \quad (2)$$

3. Results and discussion

3.1. Characterizations

The peaks at 7.32°, 10.36°, 12.7°, 14.64°, 16.38° and 18.1° in the powder X-ray diffraction (PXRD) patterns of ZIF-67@SiO_2 (Fig. 1a) could be ascribed to (011), (002), (112), (022), (013) and (222) facets of ZIF-67 (Zhang et al., 2018; Zhan and Zeng, 2017). All diffraction peaks of obtained ZIF-67@SiO_2 matched well with the pure ZIF-67, indicating that the amorphous silica shell over ZIF-67 core would not exert the influence on the structure of ZIF-67. The peak at 1061.91 cm^{-1} of ZIF-67@SiO_2 (Fig. 1b) can be assigned to the Si—O—Si bond, verifying the presence of silica (Wang et al., 2020). In addition, SEM (Fig. 2a) and TEM images (Fig. 2c) showed that ZIF-67@SiO_2 exhibited a dodecahedron shape with the particle size of approximately 600 nm, in which a core-shell structure can be clearly observed. The TAA was used as sulfur source to prepare $CoS_x@SiO_2$ using ZIF-67@SiO_2 as self-sacrificing template, and the morphology and structure of $CoS_x@SiO_2$ were characterized via FTIR, SEM, TEM, and HRTEM. No obvious PXRD diffraction peaks of $CoS_x@SiO_2$ could be observed (Fig. 1a), implying that the as-obtained $CoS_x@SiO_2$ might be amorphous (Fu et al., 2018). The characteristic peak of Si—O—Si bond at 1061.91 cm^{-1} remained after the vulcanization process (Fig. 1b), implying that SiO_2 shell exhibited an excellent stability. Meanwhile the SEM (Fig. 2b) and TEM images (Fig. 2d) showed that a two-shelled hollow nanocages with undamaged dodecahedron morphology was formed. It can be clearly observed from Fig. 2d and Fig. 3 that SiO_2 shell with a thickness of 10–20 nm was coated on hollow CoS_x to form $CoS_x@SiO_2$, which was affirmed by the uniform distribution of the elements of Co, S, Si and O.

The N_2 adsorption-desorption isotherms of both ZIF-67@SiO_2 and $CoS_x@SiO_2$ showed the typical type IV isotherm (Fig. S1), in which the presence of hysteresis loop indicated the porous structure. The ZIF-67@SiO_2 and $CoS_x@SiO_2$ exhibited a considerable specific surface area of 529.92 m^2/g and 171.47 m^2/g (Table S1), and their average pore diameters were 2.43 nm and 4.17 nm, respectively. Such a large specific surface area and mesoporous structure of $CoS_x@SiO_2$ nanocages were beneficial for providing more active sites to accelerate the SMX degradation rate.

3.2. SR-AOP catalytic activity of $CoS_x@SiO_2$

Control experiments showed that just 3% and 58% SMX were removed in 10 min by individual $CoS_x@SiO_2$ and individual PMS, respectively. SMX degradation efficiency was only 82% within 10 min when PMS was activated by ZIF-67@SiO_2 as catalyst. While, complete degradation of SMX within 6 min was realized in the presence of both $CoS_x@SiO_2$ and PMS (Fig. 4a), suggesting that PMS could be effectively activated by $CoS_x@SiO_2$ catalysts. In addition, the apparent rate constant (k_{obs}) was calculated using pseudo-first-order kinetics model to further evaluate the SR-AOP performance of $CoS_x@SiO_2$. The rate constant k of $CoS_x@SiO_2$/PMS system toward SMX degradation was 0.7286 min^{-1} (Fig. 4b), higher than those of individual $CoS_x@SiO_2$, ZIF-67@SiO_2 and PMS, respectively. As shown in Fig. S2, the total organic carbon (TOC) removal efficiencies in $CoS_x@SiO_2$/PMS system were 14.0% and 63.0% within 10 min, and 60 min, respectively. The theory calculation using Fukui function revealed that the most vulnerable sites in SMX molecule were C4, S7, N8, and N11 (Du et al., 2018), which tend to be attacked by ROSs. Based on the results of Fukui function calculation, the possible degradation pathways of SMX by $CoS_x@SiO_2$/PMS system were proposed, as shown in Fig. S3. Detailed descriptions of the SMX degradation pathways were provided in the supporting information. The above results indicated that the $CoS_x@SiO_2$ exhibited a good mineralization ability on SMX degradation.

3.3. Effects of key factors on SMX degradation in $CoS_x@SiO_2$/PMS system

3.3.1. Effect of initial pH

It was reported that initial pH can greatly affect the process of PMS activation (Hu et al., 2018). As displayed in Fig. 5a, no obvious change was observed by controlling initial pH. The SMX can be degraded completely within 6 min at a wide pH range from 2.0 to 10.0, verifying the excellent catalytic activity of $CoS_x@SiO_2$ for SMX degradation. However, considering the risk of Co leaching from CoS_x under acidic condition and the precipitation of hydroxides under alkaline condition, the optimal pH was selected to be 8.0 in the following experiments.

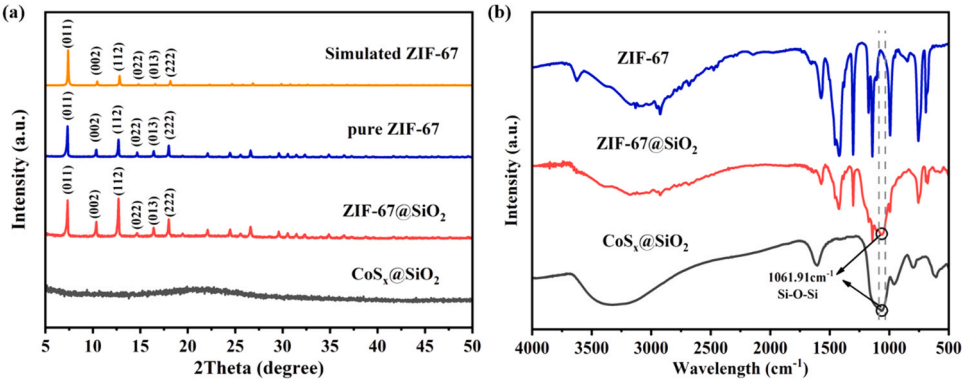

Fig. 1. (a) The PXRD patterns for simulated ZIF-67, pure ZIF-67, ZIF-67@SiO_2 and $CoS_x@SiO_2$; (b) FTIR spectra of ZIF-67, ZIF-67@SiO_2 and $CoS_x@SiO_2$.

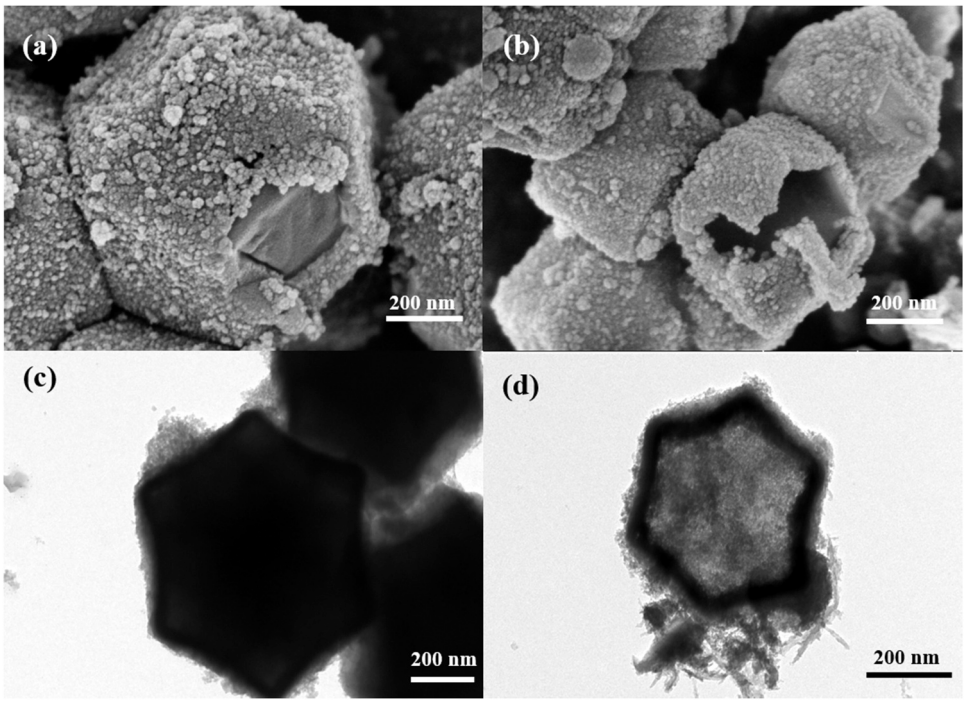

Fig. 2. The SEM images of (a) ZIF-67@SiO_2, (b) CoS_x@SiO_2; The TEM images of (c) ZIF-67@SiO_2, (d) CoS_x@SiO_2.

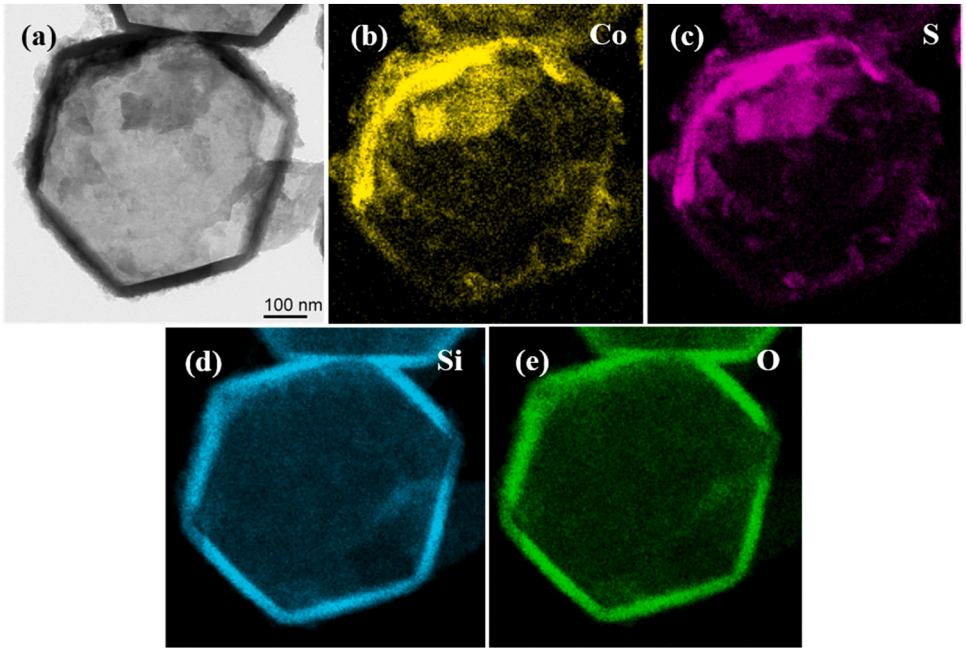

Fig. 3. (a) The HRTEM image of CoS_x@SiO_2; (b–e) The EDS elemental mapping images of CoS_x@SiO_2.

3.3.2. *Effect of PMS dosage*

PMS concentration directly determined the yield efficiencies of ROS (like $SO_4\cdot^-$, OH·, $O_2\cdot^-$ and $^1O_2$) (Yi et al., 2021). The effects of various PMS concentrations (0.1, 0.2, 0.3, 0.5 and 1.0 mM) on SMX degradation were investigated. Fig. 5b showed that the increase of the PMS dosage promoted the degradation of SMX because PMS was the source of ROS. The SMX degradation efficiency increased from 97.6% to 100% within 6 min as the PMS dosage increased from 0.1 to 0.2 mM. However, the improvement of SMX degradation efficiency was limited with the increase of PMS dosage from 0.1 to 1.0 mM due to the scavenger of excessive $SO_4\cdot^-$ by the reactions described in Eqs. (3 and 4) (Lai et al., 2018; Gao et al., 2021). Therefore, PMS dosage of 0.2 mM was selected as the optimum dosage in the subsequent experiments.

$$SO_4\cdot^- + SO_4\cdot^- \rightarrow S_2O_8^{2-} \quad (3)$$

$$HSO_5^- + SO_4\cdot^- \rightarrow SO_5\cdot^- + SO_4^{2-} + H^+ \quad (4)$$

3.3.3. *Effect of SMX concentration*

The influences of different concentrations of SMX on degradation in CoS_x@SiO_2/PMS system were also investigated (Fig. 5c). It can be

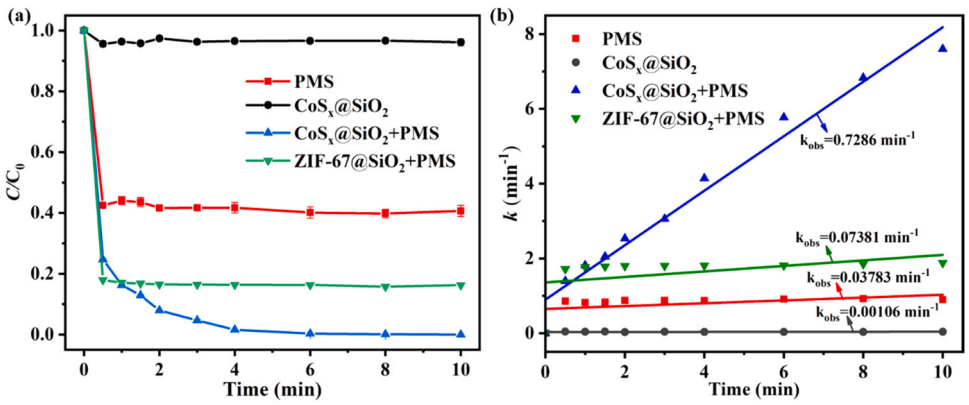

Fig. 4. (a) SMX degradation efficiency and (b) the k values over different catalysts within 10 min. Reaction conditions: SMX = 5.0 mg/L, PMS = 0.2 mM, Catalyst = 0.2 g/L, initial pH = 5.1.

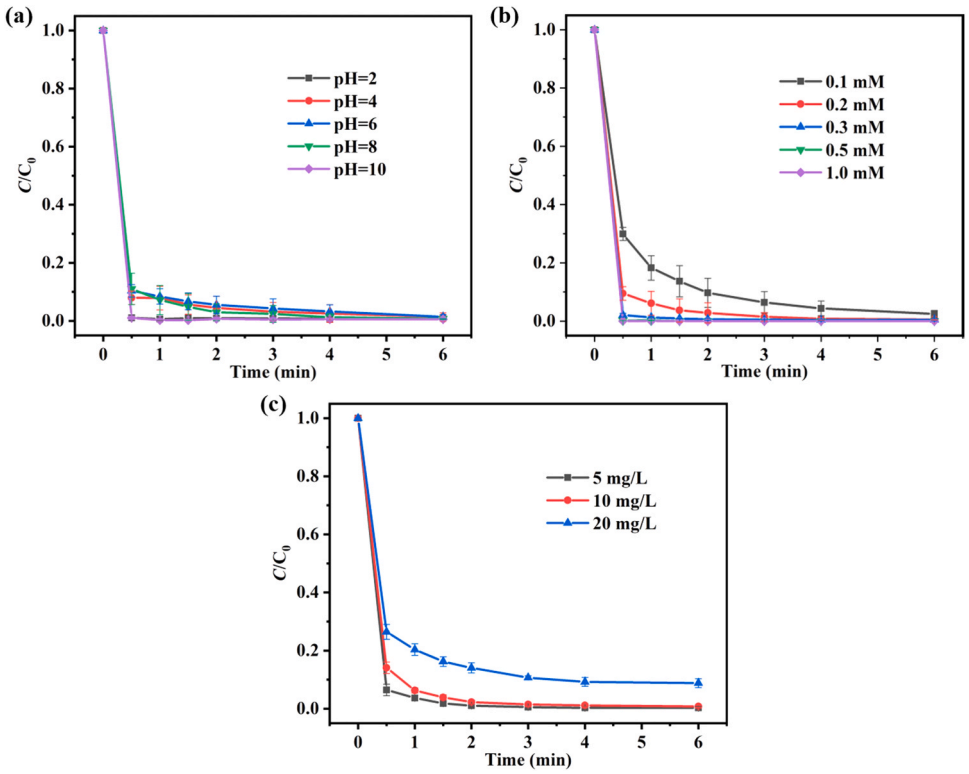

Fig. 5. Effects of (a) initial pH; (b) PMS dosage; (c) SMX concentration on SMX removal efficiency. Reaction conditions: SMX = 5 mg/L, PMS = 0.2 mM, catalyst = 0.2 g/L, initial pH = 8.0.

observed that SMX degradation efficiency decreased with the increasing of SMX concentration, which is similar to the literature (Wu et al., 2020). 100% and 94% SMX removal efficiencies were achieved with SMX concentration of 5–10 mg/L and 20 mg/L, respectively, indicating that SR-AOP activated by $CoS_x@SiO_2$ could be effective to the wide SMX concentration range. It was believed that excessive SMX cannot be degraded by the limited $SO_4^{\cdot -}$ radicals formed by the fixed addition of PMS (Li et al., 2020). Also, excessive SMX might occupy the active sites on the surface of $CoS_x@SiO_2$ to weaken the degradation performance (Lei et al., 2019).

3.3.4. *Effect of co-existing anions*

The anions like Cl^-, NO_3^- and HCO_3^- in aquatic environment could influence the degradation of pollutants (Hu et al., 2020), and the effects of these anions with the concentration of 1 mM, 10 mM and 40 mM on SMX degradation were studied (Fig. 6). Addition of Cl^- could positively enhance both the SMX removal efficiency and rate (Fig. 6a). 100% SMX decomposition efficiencies could be observed within 1.5 min in the presence of the Cl^- with different concentrations like 1 mM, 10 mM and 40 mM, which were superior to that in the reaction system without Cl^- (about 92% within 1.5 min). In the previous research, the similar result was observed by Anipsitakis et al., in which it was found that the Cl^- anions enhanced 2,4-Dichlorophenol (2,4-DCP) degradation in homogeneous Co(II)/PMS system (Anipsitakis et al., 2006). To further analyze the role of Cl^-, SMX degradation experiments were carried out without adding $CoS_x@SiO_2$. As shown in Fig. S4, SMX degradation efficiency was only 15% in 40 mM Cl^- system, while 100% SMX removal efficiency was achieved in 40 mM Cl^-/PMS system. The SMX removal efficiency in 40 mM Cl^-/PMS system was superior to that in pure PMS system (about 58%), indicating that Cl^- could react with PMS directly to yield

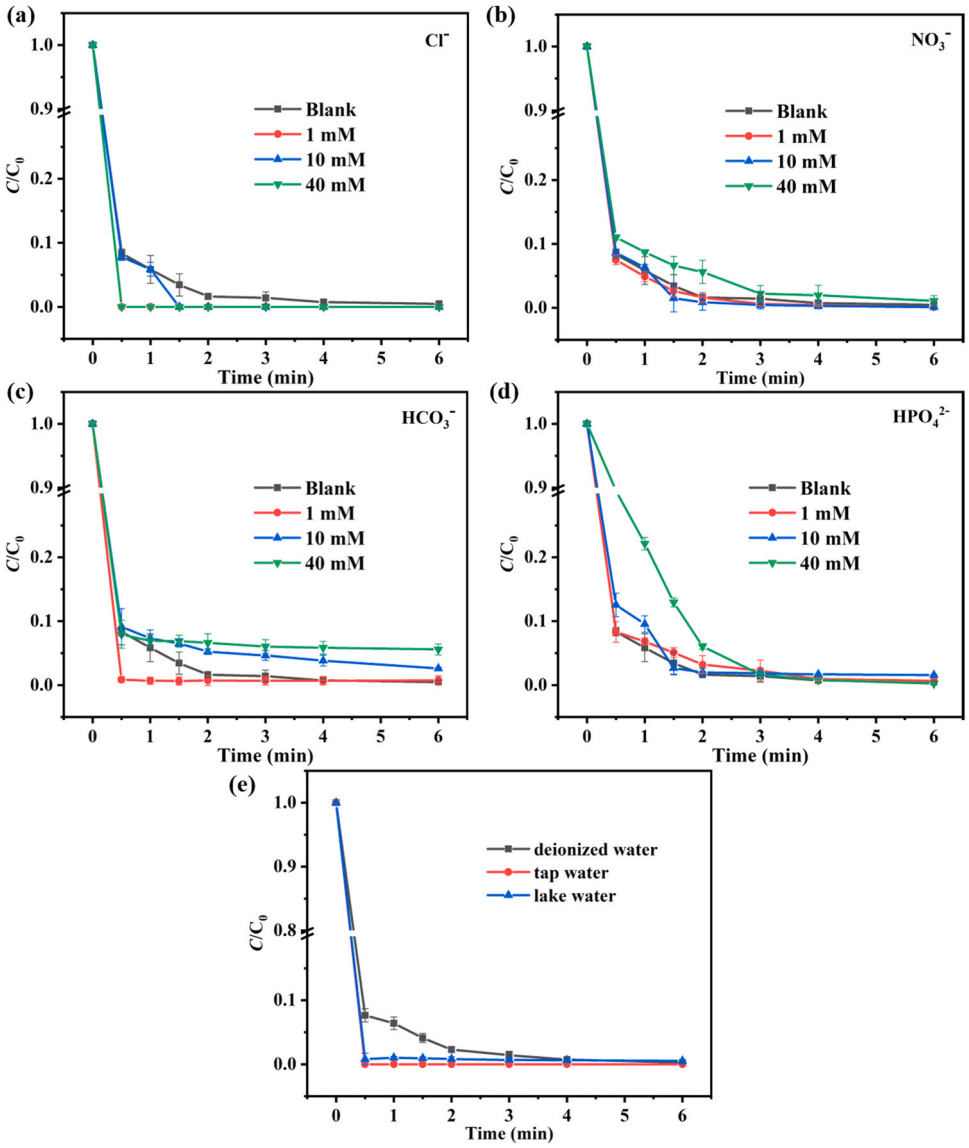

Fig. 6. The removal efficiencies of SMX in the presence of different anions, (a) Cl^-; (b) NO_3^-; (c) HCO_3^-; (d) HPO_4^{2-}; (e) The effect of different simulated wastewater on SMX removal efficiency. Reaction conditions: SMX = 5.0 mg/L, PMS = 0.2 mM, catalyst = 0.2 g/L, anions = 0–40 mM, pH = 8.0.

Cl-containing active species like HOCl to degrade SMX (Eqs. 5–8). This result matched well with the literature (Luo et al., 2019). As reported by Li's group (Luo et al., 2019), chlorinated intermediates were generated in Cl^-/PMS system, and these chlorine containing by-products were efficiently degraded in the presence of catalyst. Furthermore, the Cl-containing active species selectively degraded some specific organic pollutants, which was different from the radicals like $SO_4\cdot^-$ and ·OH. As shown in Fig. S2, it is worth to noting that about 97% TOC removal was accomplished in CoS_x@SiO_2/PMS/Cl^- system, which was significantly higher than the CoS_x@SiO_2/PMS system (about 63%). The above results indicate that Cl^- exhibited a synergistic effect in SMX degradation by CoS_x@SiO_2/PMS system.

$$Cl^- + HSO_5^- \rightarrow SO_4^{2-} + HOCl \quad (5)$$

$$2Cl^- + HSO_5^- \rightarrow SO_4^{2-} + Cl_2 + H_2O \quad (6)$$

$$Cl_2 + H_2O \rightarrow HClO + HCl \quad (7)$$

$$HClO \rightarrow H^+ + ClO^- \quad (8)$$

It can be seen from Fig. 6b that SMX degradation did not changed obviously with the addition of NO_3^-, in which just a slight inhibition effect was observed even the concentration of NO_3^- increased to 40 mM. Fig. 6c showed that low concentration (1 mM) of HCO_3^- facilitated the degradation of SMX, and 100% SMX was removed within 0.5 min. However, when the HCO_3^- concentration increased to 10 and 40 mM, the SMX degradation efficiencies decreased slightly from 100% without HCO_3^- to 97% and 95% within 6 min, respectively. As a whole, HCO_3^- played the role of two-edged sword toward the catalytic performance (Ma et al., 2018). It is reported that persulfate could react with HCO_3^- to form peroxymonocarbonate (HCO_4^-) that can enhance the removal efficiency of SMX (Jiang et al., 2017). Besides, extra H^+ generated during PMS activation would be consumed by HCO_3^-, possibly facilitating the radical generation and SMX degradation. To confirm the hypothesis, pH values before and after the catalytic reaction were measured. As shown in Fig. S5, the pH value did not change obviously with presence of low-concentration of HCO_3^-, while changed greatly without HCO_3^-, indicating that HCO_3^- acted as a buffer to maintain the pH (Guo et al., 2020b). However, the slightly decrease of SMX degradation efficiency with addition of high-concentration HCO_3^- should be attributed to the scavenger of $SO_4\cdot^-$ by excess HCO_3^- (Eqs. 9 and 10), leading to the formation of weaker radicals like $HCO_3\cdot^-$ and $CO_3\cdot^-$ (Wu et al., 2020; Xu et al., 2017; Diao et al., 2018). It can be seen from Fig. 6d that HPO_4^{2-}

did not affect SMX degradation obviously, in which 100% SMX removal efficiency was achieved within 3 min even HPO_4^{2-} up to 40 mM.

$$HCO_3^- + SO_4\cdot^- \rightarrow SO_4^{2-} + HCO_3\cdot \quad (9)$$

$$HCO_3^- + OH\cdot \rightarrow H_2O + CO_3\cdot^- \quad (10)$$

3.3.5. Effect of different simulated wastewater

To further investigate whether the $CoS_x@SiO_2$/PMS system can be used well in actual waterbody, the degradation of SMX was also carried out in tap water and lake water. The parameters of water quality of tap water and lake water were measured, as published in our previous report (Wei et al., 2021). As shown in Fig. 6e, $CoS_x@SiO_2$/PMS system showed the most outstanding degradation effect in natural water, and the SMX removal efficiency in lake water (99.5%) and tap water (100%) was higher than that in deionized water (93%) within 0.5 min. The results indicated that some common inorganic anions in natural waterbody may promote catalytic activity of the $CoS_x@SiO_2$/PMS system. As reported in previous literature (Ma et al., 2018; Wang et al., 2017), Cl^- with a low concentration (< 5 mM) played a role in degradation of pollutants. In our case, the Cl^- concentrations in lake water and tap water were 0.90 and 1.93 mM (Wei et al., 2021), respectively, which was beneficial to the improving of the SMX degradation. From the discussion above, it can be concluded that the $CoS_x@SiO_2$/PMS system is very feasible to be utilized in actual water remediation.

3.4. Catalytic mechanism of SMX degradation by PMS activation

3.4.1. Electrochemical tests

As presented in Fig. 7a, electrochemical impedance spectroscopy (EIS) of $CoS_x@SiO_2$ system showed a smaller semicircular than that of ZIF-67@SiO_2 system, indicating a lower charge-transfer resistance of $CoS_x@SiO_2$. Furthermore, the addition of PMS not only promoted the decreasing radius of the semicircular, but also accelerated the electron transfer in $CoS_x@SiO_2$/PMS system, implying that $CoS_x@SiO_2$ would be an excellent catalyst for PMS activation. Linear sweep voltammetry (LSV) curves (Fig. 7b) showed that the $CoS_x@SiO_2$+PMS+SMX system exhibited a highest current response than $CoS_x@SiO_2$, $CoS_x@SiO_2$+SMX and $CoS_x@SiO_2$+PMS systems, implying that the PMS activation and further SMX degradation occurred over $CoS_x@SiO_2$.

3.4.2. Identification and detection of ROS

The ROS ($SO_4\cdot^-$, ·OH, $O_2\cdot^-$ and $^1O_2$) could be generated by PMS activation to attack and degrade organic contaminants (Liu et al., 2021; Luo et al., 2017). To identify the dominant ROS for SMX degradation, quenching tests were carried out by adding different scavengers. Tert-butanol (TBA), BQ and L-histidine were selected as scavengers to quench ·OH, $O_2\cdot^-$ and $^1O_2$, respectively, while methanol was used to quench both $SO_4\cdot^-$ and ·OH. As shown in Fig. 8a, the SMX degradation efficiency decreased from 100% to 44.7% within 10 min when 500 mM methanol was added in, while slight decrease (from 100% to 96.5%) of SMX removal efficiency occurred using TBA as scavenger, implying that $SO_4\cdot^-$ rather than ·OH played a primary role in SMX degradation. SMX degradation efficiency decreased from 100% to 61.2% in the presence of excessive (1.0 mM) L-histidine, revealing that $^1O_2$ also played a significant role in SMX degradation. To further confirm the role of $^1O_2$, furfuryl alcohol (FFA) was selected as a specific quencher to quench $^1O_2$. As is shown in Fig. S6, the SMX degradation efficiency decreased from 100% to 33.2% when 500 mM FFA was added. Besides, β-Carotene was used as a typical scavenger to quench $^1O_2$ because it was hardly not oxidized by PMS (Luo et al., 2019). As shown in Fig. S6, the presence of β-Carotene (0.47 mM) severely inhibited the SMX degradation efficiency. These results further indicated that $^1O_2$ played an important role on SMX degradation. Moreover, no obvious decrease was observed in SMX degradation efficiency with addition of 1.0 mM BQ, demonstrating a negligible contribution of $O_2\cdot^-$ to the SMX degradation. To further confirm the existence of ROS in $CoS_x@SiO_2$/PMS system, ESR was carried out using DMPO and TEMP as spin trap agents. As shown in Fig. 8b and c, no obvious signal was observed in alone $CoS_x@SiO_2$ system, indicating that $SO_4\cdot^-$ and ·OH cannot be generated by $CoS_x@SiO_2$ itself. When PMS and $CoS_x@SiO_2$ coexisted in the SMX solution, the typical ESR signals for DMPO–$SO_4\cdot^-$ adducts and DMPO–·OH adducts appeared, and the intensity of signals become stronger as time goes on. Moreover, the characteristic signals TEMP-$^1O_2$ adducts were also detected. These results suggested that $SO_4\cdot^-$ and $^1O_2$ might be the main ROSs in $CoS_x@SiO_2$/PMS system.

Furthermore, the quantitative determination of the $SO_4\cdot^-$ generated from $CoS_x@SiO_2$/PMS system was conducted. The $SO_4\cdot^-$ radicals could react with HBA to from hydroquinone, which is immediately transformed to BQ by excess PMS (Eq. 11). The $SO_4\cdot^-$ concentration can be calculated by determining BQ (Oh et al., 2017; Buxton et al., 1988; Kurien and Robins, 1970). It can be seen from Fig. 8d that $SO_4\cdot^-$ in $CoS_x@SiO_2$/PMS system gradually accumulated as the reaction proceeded, and generated largely at the initial 0.5 min. Besides, the concentration of $SO_4\cdot^-$ increased with the increase of the ratio of HBA:PMS. However, the $SO_4\cdot^-$ production reached a plateau up to 26 μM as the ratio increase from 5:1–6:1 within 10 min. Additionally, the excess PMS with residual amount of 110 μM at the ratio of 5:1 indicated the sufficient reaction for the generation of BQ (Eq. (11)).

$$\text{HBA (excess)} + SO_4\cdot^- \rightarrow \text{hydroquinone} + \text{PMS (excess)} \rightarrow \text{BQ} \quad (11)$$

3.4.3. The role of cobalt and sulfur species

The XPS spectra showed the presence of Co 2p, S 2p, Si 2p and O 1s

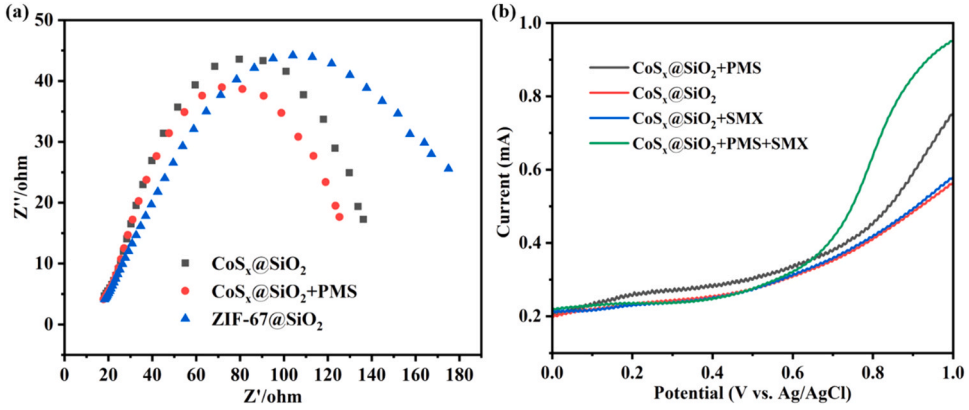

Fig. 7. (a) Electrochemical impedance spectroscopy analysis; and (b) Linear sweep voltammetry curves obtained under different conditions.

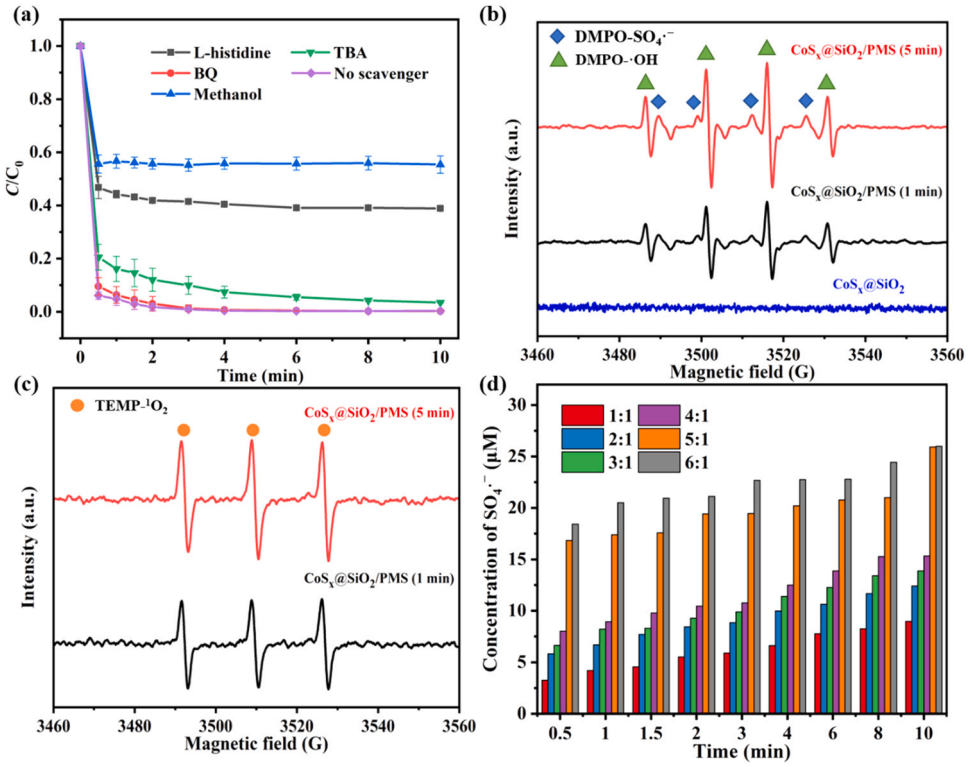

Fig. 8. (a) The reactive species quenching experiments for SMX degradation; (b) ESR spectra of DMPO-$SO_4{\cdot}^-$ and DMPO-·OH, (c) TEMP-$^1O_2$; (d) The formed $SO_4{\cdot}^-$ concentrations at different HBA: PMS ratios in CoS_x@SiO_2/PMS system.

(Fig. S7). To explore the role of Co and S in CoS_x@SiO_2/PMS system, Co 2p and S 2p XPS spectra of the CoS_x@SiO_2 were conducted. It can be seen from Fig. 9 that the positions of the peaks of the main elements in CoS_x@SiO_2 remain basically unchanged before and after the catalytic reaction. However, the chemical valence and ratio of Co and S on the surface of CoS_x@SiO_2 changed after the catalytic reaction by XPS elemental peak area analysis. As displayed in Table S2, the percentage of Co^{3+} decreased from 52.66% to 51.01% after the catalytic reaction, indicating that a part of Co^{3+} might be converted to Co^{2+} on the surface of CoS_x@SiO_2. Meanwhile, the percentages of S^{2-} and S_2^{2-} decreased from 35.5% and 33.7% to 17.8% and 24.3%, respectively, while S_n^{2-} and SO_x increased from 12.8% and 16.2% to 14.6% and 44.9%, respectively, implying that the reductive sulfur species like S^{2-} and S_2^{2-} on the surface of CoS_x@SiO_2 accelerated the regeneration of Co^{2+}.

3.4.4. Catalytic mechanism

Based on quenching tests, ESR, XPS and electrochemical tests, the possible mechanism for SMX removal in CoS_x@SiO_2/PMS system was proposed (Fig. 10). Co^{2+} could be firstly oxidized into Co^{3+} by activating PMS (HSO_5^-) to generate $SO_4{\cdot}^-$ (Eq. 12). Then, Co^{2+} was regenerated by HSO_5^- and superficial sulfur species (Eqs. 13 and 14). In other words, the presence of multivalent of sulfur species in CoS_x@SiO_2/PMS system was conducive to the conversion from Co^{3+} to Co^{2+}. Moreover, there could be other ways to generate $SO_4{\cdot}^-$ (Eqs. 15–17), in which both the S_2^{2-} and SO_3^{2-} played vital roles. $^1O_2$ was generated from the reaction between $SO_5{\cdot}^-$ and H_2O (Eq. 18) (Xu et al., 2016). Finally, the ROSs like $SO_4{\cdot}^-$ and $^1O_2$ attacked SMX to produce intermediates, even CO_2 and H_2O (Eq. 19).

$$Co^{2+} + HSO_5^- \rightarrow Co^{3+} + SO_4{\cdot}^- + OH^- \quad (12)$$

$$Co^{3+} + HSO_5^- \rightarrow Co^{2+} + SO_5{\cdot}^- + H^+ \quad (13)$$

$$Co^{3+} + S^{2-}/\ S_2^{2-} \rightarrow Co^{2+} + S_n^{2-}/SO_x \quad (14)$$

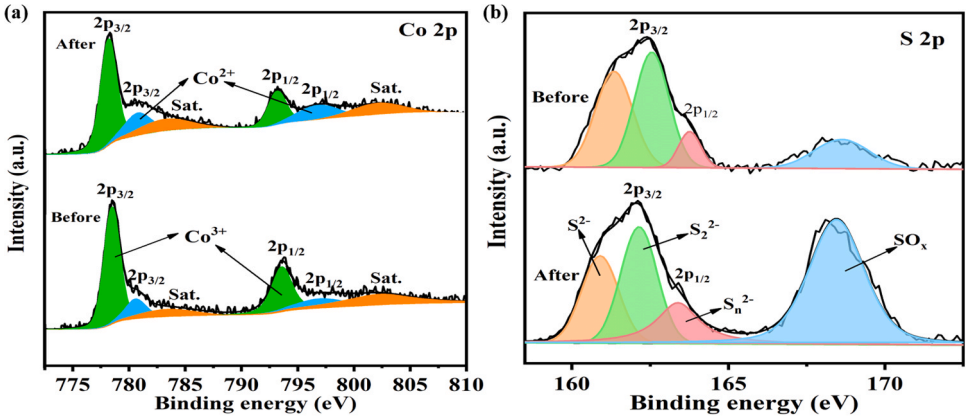

Fig. 9. (a) Co 2p and (b) S 2p XPS spectra of CoS_x@SiO_2 before and after the degradation reaction.

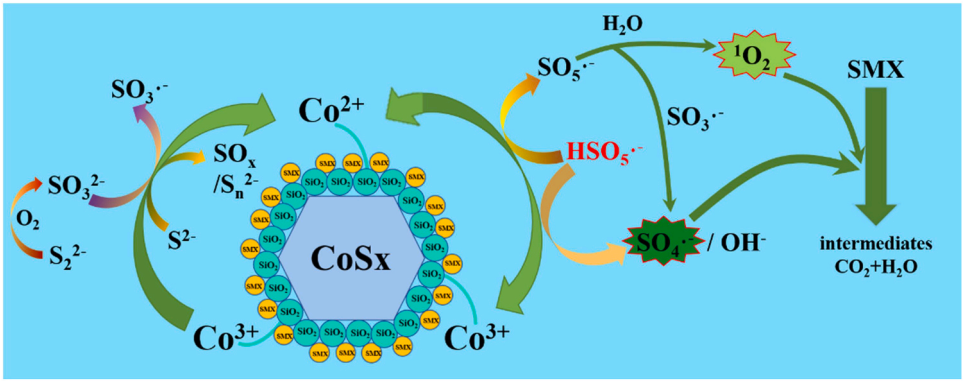

Fig. 10. Possible catalyst mechanism for SMX removal in CoS_x@SiO_2/PMS system.

$$S_2^{2-} + 3O_2 \rightarrow 2SO_3^{2-} \quad (15)$$

$$O_2 + SO_3^{2-} \rightarrow SO_5^{\cdot -} \quad (16)$$

$$SO_5^{\cdot -} + SO_3^{\cdot -} \rightarrow SO_4^{\cdot -} + SO_4^{2-} \quad (17)$$

$$2SO_5^{\cdot -} + H_2O \rightarrow 2HSO_4^{-} + 1.5\,^1O_2 \quad (18)$$

$$SO_4^{\cdot -}/\,^1O_2 + SMX \rightarrow \text{intermediates} + CO_2 + H_2O \quad (19)$$

3.5. Universality, reusability and stability of CoS_x@SiO_2

To further evaluate the potential application of CoS_x@SiO_2, the universality, reusability and stability were evaluated under the optimum conditions. 100% SMX, Sulfisoxazole (SIZ), Sulfadiazine (SDX), Bisphenol A (BPA) and Tetracycline (TC) were achieved within 10 min in the individual pollutant system with initial concentration of 5 mg/L (Fig. 11b), while ca. 99% SMX, SIZ and SDX degradation efficiencies were achieved in the co-existing pollutant system with initial concentration of 15 mg/L (Fig. S8), indicating the excellent catalytic performance of CoS_x@SiO_2 for PMS activation towards various organic pollutants. Besides, comparing with the counterpart catalysts previously reported, the CoS_x@SiO_2 nanocages exhibited superior catalytic activity on SMX degradation (Table 1). It can be seen from Fig. 11a that the SMX degradation efficiency only reached 72% within 20 min after five cycles in CoS_x/PMS system, while 100% in CoS_x@SiO_2/PMS system. The leaching Co determined by ICP-OES were 3.51 mg/L and 0.56 mg/L for individual CoS_x and CoS_x@SiO_2, respectively, verifying the protection effect of SiO_2 shell for CoS_x. As depicted in Fig. 11c and d, The PXRD pattern of the used CoS_x@SiO_2 matched perfectly with the fresh one, and the morphology of CoS_x@SiO_2 experienced no significant changes after catalytic reaction, indicating the good stability of CoS_x@SiO_2.

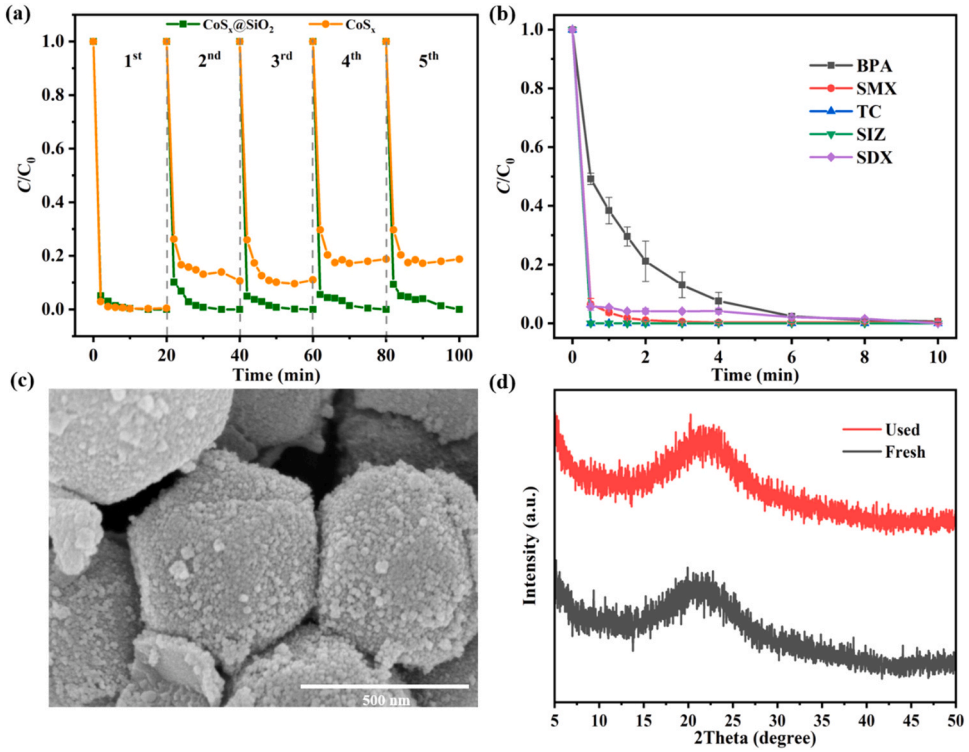

Fig. 11. (a) Consecutive runs of the catalytic activity of CoS_x@SiO_2 on SMX removal efficiency; (b) The degradation efficiency of SMX, BPA, TC, SIZ and SDX; (c) The SEM image and (d) The PXRD patterns of CoS_x@SiO_2 before and after five cycles for catalytic performance. Reaction conditions: SMX = 5 mg/L, BPA = 5 mg/L, TC = 5 mg/L, SIZ = 5 mg/L, SDX = 5 mg/L, PMS = 0.2 mM, catalyst = 0.2 g/L, initial pH = 8.0.

Table 1
Comparison of different catalyst for PMS activation.

Catalyst	Pollutant (mg/L)	PMS dosage (g/L)	Efficiency (%)	Time (min)	Ref.
CoCu LDO	SMX (10)	0.15	73.5	60	(Guo et al., 2021)
Cu_1Co_1-LDH	SMX (10)	0.144	95.2	30	(Guo et al., 2020)
CoO@mpgCN	SMX (12)	6.14	99	15	(Nguyen et al., 2021)
Co_3O_4/CC	BPA (10)	0.10	97	7	(Luo et al., 2018)
$HCCN_S$	BPA (20)	0.15	98	6	(Zhang et al., 2020)
$FeCo_2S_4$-CN	SMX (5)	0.09	91.9	15	(Li et al., 2020)
$CoFe_2O_4$-EG	SMX (10)	0.24	99	20	(Xu et al., 2019)
$CoS_x@SiO_2$	SMX (5)	0.12	100	6	This work

4. Conclusions

In all, the amorphous $CoS_x@SiO_2$ nanocage was successfully synthesized from ZIF-67 as precursor. The amorphous $CoS_x@SiO_2$ exhibited an excellent stability and high catalytic activity on the SMX degradation in a wide range of pH from 2.0 to 10.0. Under the optimum conditions (pH = 8, PMS = 0.2 mM, catalyst = 0.2 g/L, SMX = 5 mg/L), 100% SMX degradation in $CoS_x@SiO_2$/PMS system was achieved within 6 min. The Cl^- and HCO_3^- with low-concentration could facilitate the degradation of SMX, whereas the NO_3^- exerted a negligible effect on SMX removal. A possible reaction mechanism for SMX degradation in $CoS_x@SiO_2$/PMS system was explored through quenching experiments and ESR, revealing that the $SO_4^{\cdot-}$ and $^1O_2$ were the main ROS for SMX degradation in $CoS_x@SiO_2$/PMS system. In addition, the S^{2-}/S_2^{2-} in $CoS_x@SiO_2$ nanocages was beneficial for Co^{3+}/Co^{2+} recycling so that PMS could be effectively activated for SMX degradation. It was found that the presence of SiO_2 shell in $CoS_x@SiO_2$ could effectively prevent the Co leaching to improve the stability. This work will provide valuable strategy in practical treatment toward wastewater containing organic pollutants with MOF-derived materials.

CRediT authorship contribution statement

Fei Wang: Data curation, Investigation, Visualization, Writing – original draft. **Huifen Fu:** Conceptualization, Funding acquisition, Supervision, Project administration, Writing – review & editing. **Fu-Xue Wang:** Software, Methodology. **Xiu-Wu Zhang:** Software, Methodology. **Peng Wang:** Resources, Instrumental. **Chen Zhao:** Software, Methodology. **Chong-Chen Wang:** Conceptualization, Funding acquisition, Supervision, Project administration, Writing – review & editing.

Declaration of Competing Interest

The authors declare that they have no known competing financial interests or personal relationships that could have appeared to influence the work reported in this paper.

Acknowledgments

This work was supported by National Natural Science Foundation of China (22176012, 51878023, 21806008), Beijing Natural Science Foundation (8202016), Great Wall Scholars Training Program Project of Beijing Municipality Universities (CIT&TCD20180323), Beijing Talent Project (2020A27), Science and Technology General Project of Beijing Municipal Education Commission (KM202110016010) and The Fundamental Research Funds for Beijing University of Civil Engineering and Architecture (X20147/X20141/X20135/X20146).

Appendix A. Supporting information

Supplementary data associated with this article can be found in the online version at doi:10.1016/j.jhazmat.2021.126998.

References

Anipsitakis, G.P., Dionysiou, D.D., Gonzalez, M.A., 2006. Cobalt-mediated activation of peroxymonosulfate and sulfate radical attack on phenolic compounds. Implications of chloride ions. Environ. Sci. Technol. 40, 1000–1007.
Buxton, G.V., Greenstock, C.L., Helman, W.P., Ross, A.B., 1988. Critical review of rate constants for reactions of hydrated electrons, hydrogen atoms and hydroxyl radicals (·OH/·O) in aqueous solution. J. Phys. Chem. Ref. Data 17, 513–886.
Chen, L., Ji, H., Qi, J., Huang, T., Wang, C.-C., Liu, W., 2021. Degradation of acetaminophen by activated peroxymonosulfate using $Co(OH)_2$ hollow microsphere supported titanate nanotubes: insights into sulfate radical production pathway through $CoOH^+$ activation. Chem. Eng. J. 406, 126877.
Diao, Z.-H., Wei, Q., Guo, P.-R., Kong, L.-J., Pu, S.-Y., 2018. Photo-assisted degradation of bisphenol A by a novel $FeS_2@SiO_2$ microspheres activated persulphate process: synergistic effect, pathway and mechanism. Chem. Eng. J. 349, 683–693.
Ding, Y., Hu, Y., Peng, X., Xiao, Y., Huang, J., 2020. Micro-nano structured CoS: an efficient catalyst for peroxymonosulfate activation for removal of bisphenol A. Sep. Purif. Technol. 233, 116022.
Dong, C., Bao, Y., Sheng, T., Yi, Q., Zhu, Q., Shen, B., Xing, M., Lo, I.M., Zhang, J., 2021. Singlet oxygen triggered by robust bimetallic MoFe/TiO_2 nanospheres of highly efficacy in solar-light-driven peroxymonosulfate activation for organic pollutants removal. Appl. Catal. B: Environ. 286, 119930.
Duan, X., Su, C., Miao, J., Zhong, Y., Shao, Z., Wang, S., Sun, H., 2018. Insights into perovskite-catalyzed peroxymonosulfate activation: maneuverable cobalt sites for promoted evolution of sulfate radicals. Appl. Catal. B: Environ. 220, 626–634.
Du, J., Guo, W., Wang, H., Yin, R., Zheng, H., Feng, X., Che, D., Ren, N., 2018. Hydroxyl radical dominated degradation of aquatic sulfamethoxazole by Fe^0/bisulfite/O_2: kinetics, mechanisms, and pathways. Water Res. 138, 323–332.
Du, M., Yi, Q., Ji, J., Zhu, Q., Duan, H., Xing, M., Zhang, J., 2020. Sustainable activation of peroxymonosulfate by the Mo (IV) in MoS_2 for the remediation of aromatic organic pollutants. Chin. Chem. Lett. 31, 2803–2808.
Fan, Y., Ji, Y., Zheng, G., Lu, J., Kong, D., Yin, X., Zhou, Q., 2017. Degradation of atrazine in heterogeneous Co_3O_4 activated peroxymonosulfate oxidation process: kinetics, mechanisms, and reaction pathways. Chem. Eng. J. 330, 831–839.
Fu, J., Bie, C., Cheng, B., Jiang, C., Yu, J., 2018. Hollow CoS_x polyhedrons act as high-efficiency cocatalyst for enhancing the photocatalytic hydrogen generation of g-C_3N_4. ACS Sustain. Chem. Eng. 6, 2767–2779.
Gao, Y., Zhao, Q., Li, Y., Li, Y., Gou, J., Cheng, X., 2021. Degradation of sulfamethoxazole by peroxymonosulfate activated by waste eggshell supported Ag_2O-Ag nano–particles. Chem. Eng. J. 405, 126719.
Guo, R., Li, Y., Chen, Y., Liu, Y., Niu, B., Gou, J., Cheng, X., 2021. Efficient degradation of sulfamethoxazole by CoCu LDH composite membrane activating peroxymonosulfate with decreased metal ion leaching. Chem. Eng. J. 417, 127887.
Guo, R., Nengzi, L.-c, Chen, Y., Li, Y., Zhang, X., Cheng, X., 2020. Efficient degradation of sulfamethoxazole by CuCo LDH and LDH@fibers composite membrane activating peroxymonosulfate. Chem. Eng. J. 398, 125676.
Guo, R., Wang, Y., Li, J., Cheng, X., Dionysiou, D.D., 2020b. Sulfamethoxazole degradation by visible light assisted peroxymonosulfate process based on nanohybrid manganese dioxide incorporating ferric oxide. Appl. Catal. B: Environ. 278, 119297.
Hammouda, S.B., Zhao, F., Safaei, Z., Ramasamy, D.L., Doshi, B., Sillanpää, M., 2018. Sulfate radical-mediated degradation and mineralization of bisphenol F in neutral medium by the novel magnetic Sr_2CoFeO_6 double perovskite oxide catalyzed peroxymonosulfate: Influence of co-existing chemicals and UV irradiation. Appl. Catal. B: Environ. 233, 99–111.
Hu, L., Wang, P., Liu, G., Zheng, Q., Zhang, G., 2020. Catalytic degradation of p-nitrophenol by magnetically recoverable Fe_3O_4 as a persulfate activator under microwave irradiation. Chemosphere 240, 124977.
Hu, L., Zhang, G., Liu, M., Wang, Q., Wang, P., 2018. Enhanced degradation of Bisphenol A (BPA) by peroxymonosulfate with Co_3O_4-Bi_2O_3 catalyst activation: effects of pH, inorganic anions, and water matrix. Chem. Eng. J. 338, 300–310.
Jiang, M., Lu, J., Ji, Y., Kong, D., 2017. Bicarbonate-activated persulfate oxidation of acetaminophen. Water Res. 116, 324–331.
Jiang, H., Zhu, C., Yuan, Y., Yue, C., Ling, C., Liu, F., Li, A., 2020. Enhanced activation of peroxymonosulfate with metal-substituted hollow $MxCo_3$-xS_4 polyhedrons for superfast degradation of sulfamethazine. Chem. Eng. J. 384, 123302.
Ji, Y., Shi, Y., Dong, W., Wen, X., Jiang, M., Lu, J., 2016. Thermo-activated persulfate oxidation system for tetracycline antibiotics degradation in aqueous solution. Chem. Eng. J. 298, 225–233.
Ji, J., Yan, Q., Yin, P., Mine, S., Matsuoka, M., Xing, M., 2021. Defects on CoS_{2-x}: tuning redox reactions for sustainable degradation of organic pollutants. Angew. Chem. Int. Ed. 60, 2903–2908.
Kurien, K., Robins, P., 1970. Photolysis of aqueous solutions of p-benzoquinone: a spectrophotometric investigation. J. Chem. Soc. B 855–859.

Lai, L., Yan, J., Li, J., Lai, B., 2018. Co/Al_2O_3-EPM as peroxymonosulfate activator for sulfamethoxazole removal: performance, biotoxicity, degradation pathways and mechanism. Chem. Eng. J. 343, 676–688.
Lazaro, I.A., Forgan, R.S., 2019. Application of zirconium MOFs in drug delivery and biomedicine. Coord. Chem. Rev. 380, 230–259.
Lee, J., von Gunten, U., Kim, J.H., 2020. Persulfate-based advanced oxidation: critical assessment of opportunities and roadblocks. Environ. Sci. Technol. 54, 3064–3081.
Lei, X., You, M., Pan, F., Liu, M., Yang, P., Xia, D., Li, Q., Wang, Y., Fu, J., 2019. $CuFe_2O_4$@ GO nanocomposite as an effective and recoverable catalyst of peroxymonosulfate activation for degradation of aqueous dye pollutants. Chin. Chem. Lett. 30, 2216–2220.
Liu, N., Lu, N., Yu, H., Chen, S., Quan, X., 2021. Degradation of aqueous bisphenol A in the CoCN/Vis/PMS system: catalyst design, reaction kinetic and mechanism analysis. Chem. Eng. J. 407, 127228.
Li, X., Ao, Z., Liu, J., Sun, H., Rykov, A.I., Wang, J., 2016. Topotactic transformation of metal–organic frameworks to graphene-encapsulated transition-metal nitrides as efficient Fenton-like catalysts. ACS Nano 10, 11532–11540.
Li, Y.-X., Han, Y.-C., Wang, C.-C., 2020. Fabrication strategies and Cr (VI) elimination activities of the MOF-derivatives and their composites. Chem. Eng. J. 405, 126648.
Li, Y., Li, J., Pan, Y., Xiong, Z., Yao, G., Xie, R., Lai, B., 2020. Peroxymonosulfate activation on $FeCo_2S_4$ modified g-C_3N_4 ($FeCo_2S_4$-CN): mechanism of singlet oxygen evolution for nonradical efficient degradation of sulfamethoxazole. Chem. Eng. J. 384, 123361.
Li, A., Xie, L., Zhou, S., Zhang, M., Ding, Y., Wang, P., 2021. Optimization of Fe_3O_4/SiO_2/N-TiO_2/Ag/AgCl core-shell nanomaterial and its properties, repeatability and photocatalytic mechanism. J. Photochem. Photobiol. A: Chem. 409, 113141.
Li, X., Yan, X., Hu, X., Feng, R., Zhou, M., Wang, L., 2020. Hollow Cu-Co/N-doped carbon spheres derived from ZIFs as an efficient catalyst for peroxymonosulfate activation. Chem. Eng. J. 397, 125533.
Luo, R., Liu, C., Li, J., Wang, J., Hu, X., Sun, X., Shen, J., Han, W., Wang, L., 2017. Nanostructured CoP: An efficient catalyst for degradation of organic pollutants by activating peroxymonosulfate. J. Hazard Mater. 329, 92–101.
Luo, R., Liu, C., Li, J., Wang, C., Sun, X., Shen, J., Han, W., Wang, L., 2018. Convenient synthesis and engineering of ultrafine Co_3O_4-incorporated carbon composite: towards practical application of environmental remediation. J. Mater. Chem. A 6, 3454–3461.
Luo, R., Li, M., Wang, C., Zhang, M., Nasir Khan, M.A., Sun, X., Shen, J., Han, W., Wang, L., Li, J., 2019. Singlet oxygen-dominated non-radical oxidation process for efficient degradation of bisphenol A under high salinity condition. Water Res. 148, 416–424.
Ma, W., Wang, N., Fan, Y., Tong, T., Han, X., Du, Y., 2018. Non-radical-dominated catalytic degradation of bisphenol A by ZIF-67 derived nitrogen-doped carbon nanotubes frameworks in the presence of peroxymonosulfate. Chem. Eng. J. 336, 721–731.
Nguyen, T.B., Huang, C.P., Doong, R.-a, Chen, C.-W., Dong, C.-D., 2021. CoO-3D ordered mesoporous carbon nitride (CoO@mpgCN) composite as peroxymonosulfate activator for the degradation of sulfamethoxazole in water. J. Hazard Mater. 401, 123326.
Oh, W.-D., Dong, Z., Lim, T.-T., 2016. Generation of sulfate radical through heterogeneous catalysis for organic contaminants removal: current development, challenges and prospects. Appl. Catal. B: Environ. 194, 169–201.
Oh, W.D., Dong, Z., Ronn, G., Lim, T.T., 2017. Surface-active bismuth ferrite as superior peroxymonosulfate activator for aqueous sulfamethoxazole removal: performance, mechanism and quantification of sulfate radical. J. Hazard Mater. 325, 71–81.
Oh, W.-D., Lua, S.-K., Dong, Z., Lim, T.-T., 2014. High surface area DPA-hematite for efficient detoxification of bisphenol A via peroxymonosulfate activation. J. Mater. Chem. A 2, 15836–15845.
Rodenas, T., Luz, I., Prieto, G., Seoane, B., Miro, H., Corma, A., Kapteijn, F., Xamena, F.X. L. i, Gascon, J., 2015. Metal–organic framework nanosheets in polymer composite materials for gas separation. Nat. Mater. 14, 48–55.
Stassen, I., Burtch, N., Talin, A., Falcaro, P., Allendorf, M., Ameloot, R., 2017. An updated roadmap for the integration of metal–organic frameworks with electronic devices and chemical sensors. Chem. Soc. Rev. 46, 3185–3241.
Wang, Y., Cao, D., Zhao, X., 2017. Heterogeneous degradation of refractory pollutants by peroxymonosulfate activated by CoO_x-doped ordered mesoporous carbon. Chem. Eng. J. 328, 1112–1121.
Wang, C.-C., Du, X.-D., Li, J., Guo, X.-X., Wang, P., Zhang, J., 2016. Photocatalytic Cr (VI) reduction in metal-organic frameworks: a mini-review. Appl. Catal. B: Environ. 193, 198–216.
Wang, S., Wang, J., 2020. Peroxymonosulfate activation by Co_9S_8@ S and N co-doped biochar for sulfamethoxazole degradation. Chem. Eng. J. 385, 123933.
Wang, K., Xing, X., Ding, Y., Guo, W., Hong, X., Zhao, H., 2020. Resonance Raman scattering-infrared absorption dual-mode immunosensing for carcinoembryonic antigen based on $ZnO@SiO_2$ nanocomposites. Biosens. Bioelectron. 150, 111870.
Wei, X., Wang, C.-C., Li, Y., Wang, P., Wei, Q., 2021. The Z-scheme NH_2-UiO-66/PTCDA composite for enhanced photocatalytic Cr (VI) reduction under low-power LED visible light. Chemosphere 280, 130734.
Wu, X., Zhao, W., Huang, Y., Zhang, G., 2020. A mechanistic study of amorphous CoS_x cages as advanced oxidation catalysts for excellent peroxymonosulfate activation towards antibiotics degradation. Chem. Eng. J. 381, 122768.
Xu, Y., Ai, J., Zhang, H., 2016. The mechanism of degradation of bisphenol A using the magnetically separable $CuFe_2O_4$/peroxymonosulfate heterogeneous oxidation process. J. Hazard Mater. 309, 87–96.
Xu, M., Li, J., Yan, Y., Zhao, X., Yan, J., Zhang, Y., Lai, B., Chen, X., Song, L., 2019. Catalytic degradation of sulfamethoxazole through peroxymonosulfate activated with expanded graphite loaded $CoFe_2O_4$ particles. Chem. Eng. J. 369, 403–413.
Xu, Z., Shan, C., Xie, B., Liu, Y., Pan, B., 2017. Decomplexation of Cu (II)-EDTA by UV/persulfate and UV/H_2O_2: efficiency and mechanism. Appl. Catal. B: Environ. 200, 439–447.
Yan, J., Li, J., Peng, J., Zhang, H., Zhang, Y., Lai, B., 2019. Efficient degradation of sulfamethoxazole by the $CuO@Al_2O_3$ (EPC) coupled PMS system: optimization, degradation pathways and toxicity evaluation. Chem. Eng. J. 359, 1097–1110.
Yan, J., Peng, J., Lai, L., Ji, F., Zhang, Y., Lai, B., Chen, Q., Yao, G., Chen, X., Song, L., 2018. Activation $CuFe_2O_4$ by hydroxylamine for oxidation of antibiotic sulfamethoxazole. Environ. Sci. Technol. 52, 14302–14310.
Yi, X.-H., Ji, H., Wang, C.-C., Li, Y., Li, Y.-H., Zhao, C., Wang, A., Fu, H., Wang, P., Zhao, X., 2021. Photocatalysis-activated SR-AOP over PDINH/MIL-88A (Fe) composites for boosted chloroquine phosphate degradation: performance, mechanism, pathway and DFT calculations. Appl. Catal. B: Environ. 293, 120229.
Yi, Q., Tan, J., Liu, W., Lu, H., Xing, M., Zhang, J., 2020. Peroxymonosulfate activation by three-dimensional cobalt hydroxide/graphene oxide hydrogel for wastewater treatment through an automated process. Chem. Eng. J. 400, 125965.
Zhang, M., Wang, C., Liu, C., Luo, R., Li, J., Sun, X., Shen, J., Han, W., Wang, L., 2018. Metal–organic framework derived Co_3O_4/C@SiO_2 yolk–shell nanoreactors with enhanced catalytic performance. J. Mater. Chem. A 6, 11226–11235.
Zhang, M., Xiao, C., Yan, X., Chen, S., Wang, C., Luo, R., Qi, J., Sun, X., Wang, L., Li, J., 2020. Efficient removal of organic pollutants by metal–organic framework derived Co/C yolk–shell nanoreactors: size-exclusion and confinement effect. Environ. Sci. Technol. 54, 10289–10300.
Zhan, W., Sun, L., Han, X., 2019. Recent progress on engineering highly efficient porous semiconductor photocatalysts derived from metal-organic frameworks. Nano-Micro Lett. 11, 1.
Zhan, G., Zeng, H.C., 2017. ZIF-67-derived nanoreactors for controlling product selectivity in CO_2 hydrogenation. ACS Catal. 7, 7509–7519.
Zhao, C., Wang, J., Chen, X., Wang, Z., Ji, H., Chen, L., Liu, W., Wang, C.-C., 2021. Bifunctional $Bi_{12}O_{17}Cl_2$/MIL-100(Fe) composites toward photocatalytic Cr(VI) sequestration and activation of persulfate for bisphenol A degradation. Sci. Total Environ. 752, 141901.
Zhu, C., Liu, F., Ling, C., Jiang, H., Wu, H., Li, A., 2019. Growth of graphene-supported hollow cobalt sulfide nanocrystals via MOF-templated ligand exchange as surface-bound radical sinks for highly efficient bisphenol A degradation. Appl. Catal. B: Environ. 242, 238–248.